Assessing the performance of Simulated Annealing in the full inversion of dispersion velocity: Case study in the Potiguar Basin.

Alessandra Camilli Meletani and Jordi Julià, Universidade Federal do Rio Grande do Norte

Copyright 2023, SBGf - Sociedade Brasileira de Geofísica

This paper was prepared for presentation during the 18th International Congress of the Brazilian Geophysical Society held in Rio de Janeiro, Brazil, 16-19 October 2023.

Contents of this paper were reviewed by the Technical Committee of the 18th International Congress of the Brazilian Geophysical Society and do not necessarily represent any position of the SBGf, its officers or members. Electronic reproduction or storage of any part of this paper for commercial purposes without the written consent of the Brazilian Geophysical Society is prohibited.

Abstract

Inversion of surface-wave dispersion velocities has been the traditional means to determine the structure of the crust and mantle worldwide and further our knowledge on the composition and evolution of continents. Because their main sensitivity is to S-wave velocity, however, inversion approaches have generally been set to constrain this parameter alone through iterative, linearized schemes that account for partial sensitivity to P-wave velocity and density by means of empirical relationships. In this work, we assess the ability of a Simulated Annealing (SA) algorithm – a Monte Carlo search method – to simultaneously constrain all three parameters (P-velocty, S-velocity and density) during inversion. Numerical experiments suggest that the SA algorithm cannot efficiently recover all three parameters even for a simple 2-layer model, probably due to a high rejection rate during Metropolis sampling of the parameter space. Inversion of interstation group and phase dispersion curves at two broadband stations flanking the Potiguar rift were thus successful only when inverting for S-velocity with empirical constraints for P-velocity and density. Dispersion measurements were obtained in the 5 - 39 s period-range from cross-correlation and stacking of ~2 years of ambient seismic noise recordings (vertical component) with phase weighting, and the resulting velocity models displayed a thin crust (< 30 km) with S-wave velocity under 4.0 km/s consistent with a rifting environment. To further assess the plausibility of a full inversion of dispersion velocities without empirical constraints, a full mapping of the parameter space with more efficient importance sampling algorithms seems to be required.

Introduction

Surface-wave dispersion is sensitive to three parameters that define the propagation throughout an isotropic elastic medium: P-velocity, S-velocity, and density. Because the main sensitivity of dispersion velocities is to S-velocity, however, analysis of dispersion curves has consisted of constraining subsurface variations of S-velocity alone, leaving the other two parameters dependent on the first one through empirical relationships (e.g., Ritzwoller & Levshin, 1998). The objective of this study is to assess the ability of surface-wave dispersion to simultaneously determine all three parameters during inversion, which would allow for a full characterization of the subsurface without the need of several collocated geophysical surveys.

The partial sensitivity of dispersion curves to P-velocity and density can be efficiently explored through non-systematic searches of the parameter space, which form the basis of stochastic or Monte Carlo inversion methods (see, e.g., Sen & Stoffa, 1995). In particular, the Simulated Annealing approach is based on a Metropolis-Hastings sampling of the parameter space, where the acceptance or rejection of a candidate point in parameter space depends on the point explored in the previous step. This importance sampling approach results in a selective and efficient mapping of the parameter space, allowing for a feasible exploration of a large number of parameters. The Simulated Annealing algorithm – which is inspired by the physical annealing of metals – assumes a Boltzmann distribution, where the root-mean-square (RMS) difference between observations and predictions takes the role of energy and temperature is decreased by means of a prescribed annealing schedule that drives the process to an absolute energy minimum (Kirkpatrick et al., 1983). At the beginning of the inversion process, the model space is explored in an almost undirected way that avoids entrapment by local minima; as temperature decreases, however, importance sampling takes over and trial solutions are guided towards the energy minimum (Menke, 2012).

Our region of interest is the Potiguar basin, an aborted rift basin along the Equatorial margin of South America that formed in the Cretaceous. According to Matos (1992), the basin includes an off-shore portion made of asymmetric grabens resulting from the opening of the Equatorial Atlantic, and an on-shore portion consisting of extensional faults and NE-SW oriented half-grabens, originated from the formation of the opening of the South Atlantic Ocean. The sedimentary rocks of the on-shore portion are located on top of the crystalline basement rocks making the Borborema Province, a remnant of a larger Neoproterozoic mobile belt crisscrossed by an extensive network of shear zones that likely controlled fault development during rifting (Almeida et al.,1981; De Castro et al., 2012). Since the Potiguar basin is located on a low-seismicity portion of the South American plate (e.g. Ferreira et al., 1998), the study of the underlying velocity and density structure is better achieved through passive seismic interferometry. Seismic interferometry was initially introduced by Shapiro and Campillo (2004), who demonstrated that the surface-wave response of the propagating medium emerges from cross-correlation and

stacking of diffuse or random wavefields such as the ambient seismic noise wavefiled.

The data used in this study was collected by the Laboratório Sismológico of the Universidade Federal do Rio Grande do Norte (LabSis/UFRN), with funding from the national oil company PETROBRAS, with the purpose of studying the architecture of syn-rift zones in the Brazilian Northeast. In the Potiguar Basin, a total of 7 seismic stations (2 broadband and 5 short-period) were deployed between 2018 to 2020, recording continuously at a rate of 100 samples per second. Here, we considered data from the two broadband stations, which were located in Macau (MCAU) and Mossoró (MOSS), close to the main faults flanking the Potiguar rift.

Green's Functions Retrieval

Following Wapenaar et al. (2010), passive seismic interferometry uses cross-correlation of ambient seismic noise recorded at two locations to reconstruct the seismic response between those two locations. The cross-correlation between the two receivers cancels the traveltime along the common portion of the source-station path, leaving a signal as if a virtual source emitted at one location (x_A) were recorded by a receiver at the other location (x_B). Realize that, in this case, the travel time along the common path, the propagation velocity c, the position of the actual source (x_S), and the absolute time (t_S) at which it is emitted need not be known. Representing the cross-correlation by an asterisk, we can describe the cross-correlation as

$$G(x_B, x_A, t) = G(x_B, x_S, t) * G(x_A, x_S, -t), \qquad (1)$$

where $G(x_B,x_S,t)$ and $G(x_A,x_S,–t)$ represent the Green's function between source and receiver, and $G(x_B,x_A,t)$ represents the Green's function between the two receivers. As an illustration, if an impulsive source were considered, then $G(x_A,x_S,t) = \delta(t - t_A)$, with $t_A = (x_A - x_S)/c$, $G(x_B,x_S,t) = \delta(t - t_B)$, with $t_B = (x_B - x_S)/c$, and $G(x_B,x_A,t) = \delta(t - (t_B-t_A))$. Thus, the cross-correlation displaces the impulsive source in time an amount equal to the travel time between x_A and x_B, effectively turning the cross-correlation into the Green's function between those two locations.

In practice, seismic recordings need to be pre-processed before cross-correlograms are developed. First, the vertical component of the seismic recordings is cut into one day-long windows, and the resulting time series are then demeaned, detrended and low-pass filtered below 0.4 Hz, to avoid aliasing before being resampled to 10 samples per second. Following Bensen et al. (2007), a one-bit temporal normalization is next applied in the time domain to each of the one day-long segments to minimize the signature of earthquakes, and spectral whitening is subsequently applied to equalize the importance of every frequency in the signal spectrum (Bensen et al., 2007). Finally, cross-correlations are computed for each pair of one day-long segments and stacked to improve signal-to-noise ratio. In particular, we used the geometrically normalized cross-correlation (Schimmel and Paulssen, 1997), which efficiently normalizes the amplitudes of the cross-correlograms, and stack with phase weight (Schimmel & Paulssen, 1997) to avoid amplification of incoherent signals. The results of the Green's Function retrieval between stations MCAU and MOSS are displayed in the top panels of Figure 1. Figure 1a displays six Green's functions obtained after a stack of an increasing number of randomly selected days. It is clear that only the causal portion of the Green's functions displays a signal, with no relevant amplitude being displayed on the acausal portion. The random stacks also suggest that convergence is achieved after just 100 days. This is confirmed in Figure 1b, which displays the similarity between random stacks and the full stack of all 638 one day-long correlograms; a close inspection of Figure 1b reveals that similarity is close to 1 after just 100 days.

Dispersion Measurement

Group and phase dispersion velocities are measured on the reconstructed EGFs through the Automated Frequency-Time Analysis (AFTAN) of Levshin et al. (1989). In brief, the AFTAN approach consists of building the 'analytic signal' of a set of narrow, low-pass filtered versions of the raw signal, using Gaussian filters centered at a range of central frequencies (ω0). This results is a complex-valued function in the time-frequency domain, for which a smooth amplitude envelope (|A(t,ω0)|) and phase (φ(t,ω0)) can be obtained. Group velocities can then be obtained from the maximum of the envelope function, while phase velocities can be obtained from the corresponding phase function (Levshin et al., 1989). Phase was measured at the group-delay arrival time, using an average phase-velocity curve for the Borborema Province (Almeida et al., 2015) to resolve phase ambiguity and a zero phase-source term appropriate for noise sources (Bensen et al., 2007).

Dispersion measurements for the EGF between stations MCAU and MOSS are displayed in the bottom panels of Figure 1. Note that, as the cross-correlograms were obtained with vertical recordings, the surface-wave signal recovered by the EGF corresponds to a Rayleigh wave. Figure 1c shows the dispersion curves and confidence bounds for the EGF obtained from the full stack of one day-long correlograms (black), along with dispersion curves for EGFs obtained from the stacking of a random number of days (color) displayed in Figure 1a. It is clear that dispersion curves converge after stacking of 100 days at short periods (< 15 s), but that long periods require stacking of a larger number of days. Figure 1d shows the AFTAN amplitude surface for the full stack EGF.

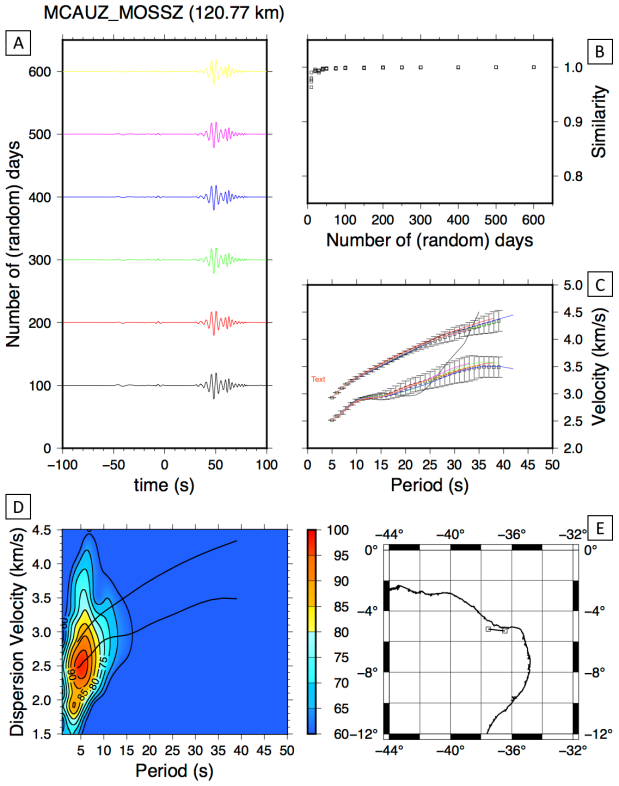

Figure 1 *– Green's function computation and group and phase velocity measurement between stations MCAU and MOSS. (A) Stacks of one day-long correlograms for an increasingly larger number of randomly selected days; (B) Similarity between randomly stacked correlograms and a full stack of all available one day-long correlograms; (C) Dispersion curves for the random stacks shown to the left (color) superimposed to the dispersion curves for the full stack (black) with 1-s confidence bounds computed from all possible 3-month stacks; (D) AFTAN surface with phase and group velocities superimposed; (E) Map displaying the ray-path between stations MCAU and MOSS.*

Inversion of Dispersion Velocities

To obtain estimates of P- and S-wave velocity and density from Rayleigh-wave dispersion, we considered a Simulated Annealing (SA) approach (e.g. Sen and Stoffa, 1995). This is a non-systematic search algorithm that explores the parameter space through importance sampling, while forcing the search to converge to an optimal solution. Through use of a Metropolis-Hastings sampler, the algorithm generates a random set of samples in the parameter space that follow a Boltzmann probability density function (pdf) that mimics the annealing process in metals. The Boltzmann pdf is defined as

$$p(x) = e^{-\frac{E(m)}{T}}, \qquad (2)$$

where E is energy and T is temperature. In that function, energy is replaced by the root-mean-square (RMS) misfit between observations and predictions and temperature is slowly reduced through a prescribed annealing schedule given as

$$T_k = 0,1 \cdot E_0 \left(\frac{N-k+1}{N}\right)^2, \qquad (3)$$

where E_0 is the RMS for the initial sample, T_k is the temperature for the *k-th* iteration, and N is the total number of iterations, until a stable (optimal) solution that minimizes energy is found. The benefits of the Metropolis-Hastings sampler is that it only requires knowledge of a function *f(x)* proportional to the true pdf, and that it makes use of Markov chains (where each trial solution depends on the previous one). Once a new trial sample is generated, it will be accepted when the RMS misfit is reduced and conditionally accepted when it is not, thus avoiding entrapment around local minima in the misfit surface.

Before inverting the dispersion measurements obtained in the previous section, a number of numerical experiments were implemented to assess SA performance. We first considered a 3 layer over a half-space model mimicking a sedimentary layer over a 2-layer crust on top of a half-space mantle (Table 1), and computed phase and group velocities for the fundamental mode of Rayleigh waves. We considered periods between 5 and 50 s, which are close to the period range in which our EGF seems to provide reliable measurements. The results of the numerical experiments are displayed in Figure 2, showing that even after 10^9 trial solutions the SA algorithm did not converge to the true solution. We then removed the layer of sediments to reduce the size of the parameter space, and run the SA inversion again. The results are displayed also in Figure 2. Although the optimal solution seems to be closer to the true solution, convergence is still not achieved. Note that, for all SA inversions, the search of the parameter space was performed within the bounds given in Table 1.

Table 1 *–True velocity model and parameter space bounds*

True Model			
P-velocity (km/s)	S-velocity (km/s)	Density (g/cm^3)	Thickness (km)
5.0000	2.6726	2.3700	1.5000
6.3000	3.6373	2.7860	13.500
6.7000	3.8682	2.9140	25.000
8.1000	4.6765	3.3620	0.0000
Parameter Space Bounds			
P-velocity (km/s)	S-velocity (km/s)	Density (g/cm^3)	Thickness (km)
4.0 - 6.0	2.0 - 3.0	2.0 - 3.0	0.5 - 2.5
6.0 - 6.5	3.0 - 4.0	2.5 - 3.0	10 - 30
6.5 - 7.5	3.5 - 4.5	2.7 - 3.0	10 - 30
7.5 - 8.5	4.0 - 5.0	3.2 - 3.5	0 - 0

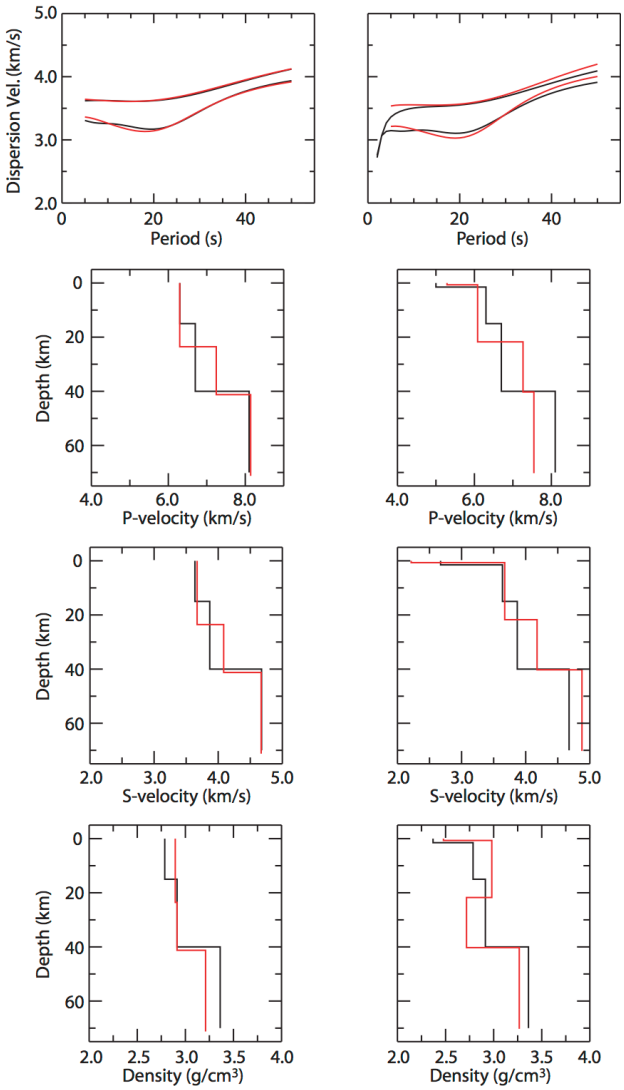

Figure 2 *– SA inversion results for a 2-layer over half-space (left) and a 3-layer over half-space (right) model. Top panels display true (black) and inverted (red) dispersion curves, while the remaining panels display true (black) and inverted (red) models for P-velocity, S-velocity, and density.*

Better results were achieved when inverting for S-velocity and layer thickness only, with calculation of P-velocity from an assumed Vp/Vs ratio and density from empirical relationships. Results for this numerical experiment are displayed in Figure 3, showing that convergence is achieved for the 2-layer over half-space case. For the 3-layer case convergence the inversion process gets close to convergence, but noticeable discrepancies do exist between observed and true models.

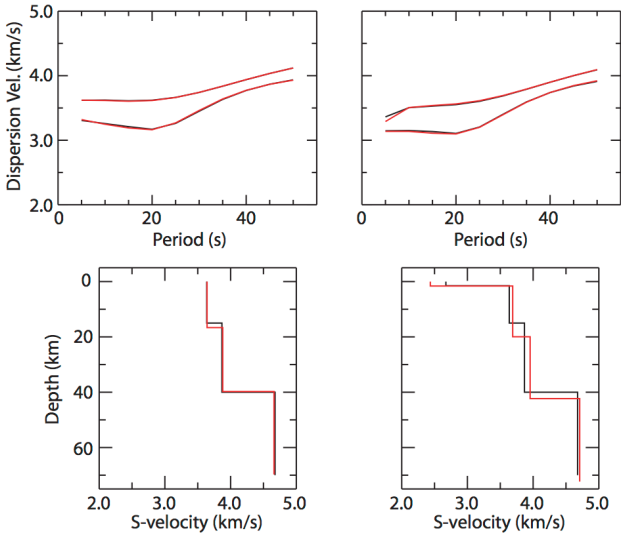

Figure 3 *– SA inversion results for a 2-layer over half-space (left) and a 3-layer over half-space (right) model. Only S-velocity and layer thickness were inverted for. Top panels display true (black) and inverted (red) dispersion curves, while bottom panels display true (black) and inverted (red) models for S-velocity.*

Somewhat disappointingly, the numerical experiments demonstrate that proximity to the true model is only achieved when searching for S-velocity and layer thickness only, with a priori constraints for the other parameters. As discussed later, the Metropolis-Hastings sampler is known to have a high-rejection rate of trial solutions, which might make it inefficient for retrieving all physical parameters at the same time.

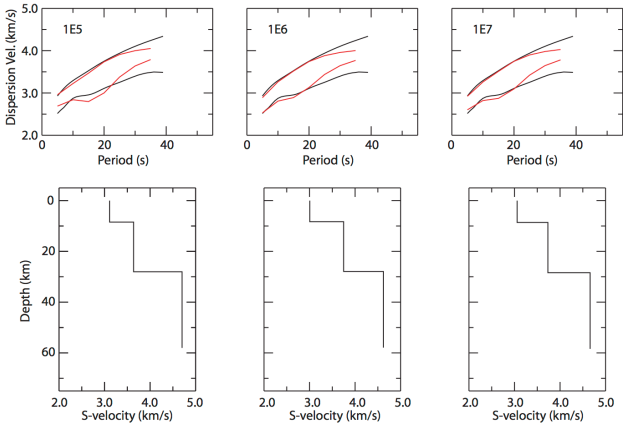

Figure 4 *– Inversion results for the inversion of the EGF between stations MCAU and MOSS for an increasing number of trial models (1E5 to 1E7). Top panels display the match between observed (black) and inverted (red) dispersion curves, while bottom panels display the inverted S-velocity models. Note the similarity among the inverted models regardless of the number of trials.*

Finally, the inversion results for the dispersion measurements developed from the EGF between MCAU and MOSS are displayed in Figure 4. The inverted model is characterized by an 8.5 km thick upper crust of 3.1 km/s, a 20 km thick lower crust with S-velocity around 3.7 km/s and an upper mantle of 4.6 km/s. Note that the match between observations and predictions is good for periods below 25 s, implying that upper mantle velocities are probably not reliable. Also note that crustal thickness is less than 30 km in total.

Discussions

In this study, we focused on the inversion of surface-wave dispersion velocities to simultaneously constrain P-velocity, S-velocity, and density. However, the results obtained using Simulated Annealing revealed limitations in efficiently recovering all three parameters, even for a simple 2-layer model over a half-space. Our guess is that the SA approach had difficulties in finding a solution when inverting for all three parameters either because of a high rejection rate during the Metropolis-Hastings sampling of the space parameter, broad valleys in the RMS misfit surface around true P-velocity and density when compared to S-velocity, or both. Building marginal probability density functions for the even simpler 1-layer over half-space might help discriminate between the two aforementioned possibilities, as such a reduced-size parameter space could be explored through a systematic grid-search. At any rate, future improvement of the inversion procedure will require sampling the parameter space with other Markov Chain Monte Carlo algorithms, such as the Gibbs sampler (e.g. Sambridge and Mosegaard, 2002), and testing other global optimization approaches such as Genetic Algorithms or the Neighborhood Algorithm (Sen and Stoffa, 1995). Gaining a better understanding of the parameter space might help design a more efficient inversion strategy.

While this study focused on the inversion of Rayleigh waves, it would be beneficial to include estimates for Love wave dispersion velocities in future investigations. By incorporating both dispersion types, additional constraints on subsurface structure would be provided that might help guide the MCMC sampling towards a stable solution. In any case, inversion of Rayleigh-wave dispersion alone provided estimates of crustal thickness that are consistent with those reported in Barbosa et al. (2023) for stations MCAU and MOSS from receiver function analysis; while we obtain a crustal thickness of 28.5 km, receiver functions estimates were around 28.4±0.5 km and 27.7±1.1 km for MCAU and MOSS, respectively. Moreover, crustal S-wave velocities were reported under 4.0 km/s in Barbosa et al. (2023), consistent with our velocity models (Figure 4).

Conclusions

This study focuses on the inversion of Rayleigh wave phase and group velocities obtained from cross-correlation of 638 days of ambient seismic noise recorded at stations MCAU and MOSS, flanking the Potiguar rift of the onshore Potiguar basin. Daily cross-correlations were performed on the vertical component and stacked with phase weighting, to then measure dispersion at periods between 5 and 39 s. To invert for Earth structure, a Simulated Annealing algorithm was implemented. Initial attempts to simultaneously determine P-velocity, S-velocity and density were unsuccessful, probably due to inefficient sampling of the parameter space; inversions for S-velocity with a priori constraints for P-velocity and density were - as expected - more successful. The inverted velocity model revealed a thin crust of less than 30 km and crustal velocities under 4.0 km/s, which are consistent with results from an independent receiver function study in the region. Future work will contemplate addition of Love-wave dispersion velocities and use of other global optimization methods and importance sampling algorithms for inversion.

Acknowledgments

Data was acquired through funding from the national oil company Petrobras (grant number 5850.0106463.17.9). Research facilities were provided by the *Laboratório de Sismologia* (LabSis) and *Departamento de Geofísica* (DGEF) of the *Universidade Federal do Rio Grande do Norte* (UFRN). ACM thanks the *Sociedade Brasileira de Geofísica* (SBGf) for awarding a scholarship that supported her research activities within this study. JJ thanks the Conselho Nacional de Desenvolvimento Científico e Tecnológico (CNPq) for his research fellowship (CNPq-308644/2019-0).

References

ALMEIDA, F. F. M., HASUI, Y., DE BRITO NEVES, B. B., & FUCK, R. A. 1981. Brazilian structural provinces: an introduction. *Earth-Science Reviews*, 17(1-2), 1-29.

ALMEIDA, Y. B. M. M., JULIÀ, J., & FRASETTO, A. 2015. Crustal architecture of the Borborema Province, NE Brazil, from receiver function CCP stacks: Implications for Mesozoic stretching and Cenozoic uplift. Tectonophysics, 649, 68-80.

BARBOSA, T. S. G., JULIÀ, J., & NASCIMENTO, A. 2023. Lithospheric S-velocity structure of the on-shore Potiguar Basin, NE Brazil: High heat-flow in an aborted rift. *Journal of Geodynamics*, 155, 101952.

BENSEN, G. D., RITZWOLLER, M. H., BARMIN, M. P., LEVSHIN, A. L., LIN, F., MOSCHETTI, M. P., SHAPIRO, N. M., & YANG, Y. 2007. Processing seismic ambient noise data to obtain reliable broad-band surface wave dispersion measurements. *Geophysical Journal International*, 169(3), 1239-1260.

DE CASTRO, D. L., BEZERRA, F. H., SOUSA, M. O., & FUCK, R. A. 2012. Influence of Neoproterozoic tectonic fabric on the origin of the Potiguar Basin, northeastern Brazil and its links with West Africa based on gravity and magnetic data. *Journal of Geodynamics*, 54, 29-42.

FERREIRA, J. M., OLIVEIRA, T., TAKEYA, M. K., & ASSUMPÇÃO, M. 1998. Superposition of local and regional stresses in northeast Brazil: evidence from focal mechanisms around the Potiguar marginal basin. *Geophysical Journal International*, 134(2), 341-355.

KIRKPATRICK, S., GELATT JR, C. D., & VECCHI, M. P. 1983. Optimization by simulated annealing. *Science*, 220(4598), 671-680.

LEVSHIN, A. L., YANOVSKAYA, T. B., LANDER, A. V., BUKCHIN, B. G., BARMIN, M. P., RATNIKOVA, L. I., & ITS, E. N. 1989. Seismic Surface Waves in a Laterally Inhomogeneous Earth, Kluwer Academic.

MATOS, R. M. D. 1992. The northeast Brazilian rift system. *Tectonics*, 11(4), 766-791.

MENKE, W. 2012. Geophysical data analysis: discrete inverse theory: MATLAB edition (Vol. 45). Academic Press.

SAMBRIDGE, M., & MOSEGAARD, K. 2002. Monte Carlo methods in geophysical inverse problems. *Reviews of Geophysics*, 40(3), 3-1.

RITZWOLLER, M. H., & LEVSHIN, A. L. 1998. Eurasian surface wave tomography: Group velocities. *Journal of Geophysical Research: Solid Earth*, 103(B3), 4839-4878.

SCHIMMEL, M., & PAULSSEN, H. 1997. Noise reduction and detection of weak, coherent signals through phase-weighted stacks. *Geophysical Journal International*, 130(2), 497-505.

SEN, M. K., & STOFFA, P. L. 1995. Global optimization methods in geophysical inversion. Cambridge University Press.

SHAPIRO, N. M., & CAMPILLO, M. 2004. Emergence of broadband Rayleigh waves from correlations of the ambient seismic noise. *Geophysical Research Letters*, 31(7).

WAPENAAR, K., DRAGANOV, D., SNIEDER, R., CAMPMAN, X., & VERDEL, A. 2010. Tutorial on seismic interferometry: Part 1—Basic principles and applications. *Geophysics*, 75(5), 75A195-75A209.